

Electron magnetic resonance study in a single crystal of the colossal magnetoresistance manganite $\text{Nd}_{0.5}\text{Sr}_{0.5}\text{MnO}_3$

S. Angappane, M. Pattabiraman, G. Rangarajan,* and K. Sethupathi
Department of Physics, Indian Institute of Technology, Madras, Chennai-600 036, India

V. S. Sastry

Materials Science Division, Indira Gandhi Centre for Atomic Research, Kalpakkam 603 102, India
 (Received 19 February 2003; revised manuscript received 5 January 2004; published 30 March 2004)

We report here the results of an electron magnetic resonance study of a single crystal of the CMR manganite, $\text{Nd}_{0.5}\text{Sr}_{0.5}\text{MnO}_3$. The temperature dependence of the paramagnetic g -value, the linewidth, and the intensity point to the existence of orbitally ordered short-ranged spin correlations. The magnetocrystalline anisotropy of the sample is found to split the spectra below T_C . The temperature dependence of the spectra and the angular variation of the resonance fields suggests the presence of two distinct anisotropy fields below 220 K. This is attributed to the coexistence of an A -type antiferromagnetic phase with the ferromagnetic phase down to the temperature at which a transition takes place to a charge ordered CE-type antiferromagnetic state ($T_{CO}=T_N=148$ K).

DOI: 10.1103/PhysRevB.69.094437

PACS number(s): 75.47.Lx, 76.30.-v, 76.50.+g

I. INTRODUCTION

Rare-earth manganese perovskites (RMnO_3 ; $R = \text{La, Nd, Pr, } \dots$) when doped with alkaline earths ($\text{R}_{1-x}\text{A}_x\text{MnO}_3$; $A = \text{Ca, Sr, Ba, } \dots$) ($0.2 \leq x \leq 0.4$) exhibit colossal magnetoresistance (CMR) and an insulator-to-metal transition concomitant with a paramagnetic to ferromagnetic transition.¹ When the doping concentration is increased to $x = 0.5$, the ferromagnetic metallic phase, upon cooling, undergoes another transition at lower temperatures to an antiferromagnetic insulating phase, accompanied by a real-space ordering of the $d_{3x^2-r^2}$ and $d_{3y^2-r^2}$ orbitals and the Mn^{3+} and Mn^{4+} ions in a checkerboard pattern,² resulting in a doubling of the unit cell along the a axis. This state, referred to as the correlated electronic (CE) state, is composed of zigzag ferromagnetic chains of Mn^{3+} and Mn^{4+} coupled antiferromagnetically in a direction perpendicular to the zigzag arrays.

For $\text{Nd}_{0.5}\text{Sr}_{0.5}\text{MnO}_3$ (NSMO 0.5), the paramagnetic insulator to ferromagnetic metal transition is observed at ($T_C =$) 250 K and upon further cooling, the transition to the CE state is observed at ($T_{CO} =$) 150 K. A number of experimental studies³ suggest that the CE state is inhomogeneous. For example, a transmission electron microscopy study of NSMO 0.5 as a function of temperature⁴ points to the coexistence of ferromagnetic metallic regions and charge ordered (CO) microdomains in the ferromagnetic state. ^{55}Mn NMR measurements in $\text{La}_{0.5}\text{Ca}_{0.5}\text{MnO}_3$ (Ref. 5) and NSMO 0.5 (Ref. 6) confirm the existence of a ferromagnetic phase fraction below T_{CO} .

Recently, using neutron diffraction, Ritter *et al.*⁷ reported the coexistence of A -type antiferromagnetic (AFM) (ferromagnetic planes coupled antiferromagnetically) and ferromagnetic phases below 225 K in NSMO 0.5. The A -type AFM phase is found to persist down to liquid helium temperatures in NSMO 0.5 and has not been observed in $\text{La}_{0.5}\text{Ca}_{0.5}\text{MnO}_3$.

We report here an electron spin resonance (ESR) study in single crystals of NSMO 0.5 with the aim of studying the temperature evolution of the magnetically ordered phases. Such a study is important in order to understand the evolution of the A -type orbitally ordered phase as a function of composition x in $\text{Nd}_{1-x}\text{Sr}_x\text{MnO}_3$. For example, for $x = 0.55$, the CE state is not observed and only the A -type AFM phase is observed ($T_N = 230$ K). For $0.3 \leq x \leq 0.5$, x-ray synchrotron⁸ measurements, indicate the existence of charge or orbitally ordered clusters.

We have previously reported the existence of spin clusters in polycrystalline $\text{Nd}_{1-x}\text{Sr}_x\text{MnO}_3$ ($0.2 \leq x \leq 0.5$) in the paramagnetic state.⁹ The formation of clusters in the paramagnetic state was evidenced by a quasilinear increase of the ESR linewidth (ΔH_{pp}) as the temperature was increased above T_C . At a characteristic temperature T^* , which is well above T_C , the line could be resolved into two Lorentzians in the magnetically ordered phase, indicating the existence of two types of phase-segregated regions. In the case of polycrystalline NSMO 0.5 the second line, which appears below T^* , shifts to higher fields.

II. EXPERIMENTAL DETAILS

Single crystal of NSMO 0.5 used in this study was grown in an infrared image furnace by the floating zone technique at the Department of Physics, University of Warwick, UK and was characterized by x-ray diffraction, dc electrical resistivity and magnetization measurements.

Single-crystal x-ray diffraction data were collected using an Enraf-Nonius CAD-4 diffractometer.¹⁰ A small crystal of dimensions $0.1 \times 0.1 \times 0.075$ mm was used for data collection. The unit-cell parameters were determined using 25 reflections collected through search routine and indexed using the method of short vectors followed by least-squares refinement. The intensity data were collected by ω - 2θ scan technique for $2^\circ < \theta < 25^\circ$ with graphite monochromated MoK_α (0.71073 \AA) x-ray radiation. The empirical absorption cor-

TABLE I. Lattice parameters and list of derived atomic positions and equivalent isotropic displacement parameters of the $\text{Nd}_{0.5}\text{Sr}_{0.5}\text{MnO}_3$ single crystal.

Lattice parameters:				
$a = 5.420(3) \text{ \AA}$, $b = 7.666(7) \text{ \AA}$, $c = 5.453(10) \text{ \AA}$				
Atoms	x	y	z	$U(\text{eq})$
Nd	0	0.25	0.0039(3)	0.021(2)
Sr	0	0.25	0.0039(3)	0.021(2)
Mn	0	0	0.5	0.018(3)
O(1)	0	0.25	0.524(5)	0.044(7)
O(2)	0.25	0.0229(18)	0.75	0.037(5)

rection was effected on the intensity data using ψ -scan technique.¹¹ The structure solution was carried out using the computer program SIR92 and the structure was refined using SHELXL-97 computer program.^{12,13} The refinement of the crystal structure was performed with full occupancies for Mn, O(1), and O(2). The occupancies of Nd and Sr were set as least-squares variables with sum of their occupancies restrained to one. The refinement converged to a final R factor of 4.9%.¹⁴ The lattice parameters, atomic positions, and equivalent isotropic displacement parameters $U(\text{eq})$ are shown in Table I. Figure 1 shows the unit cell of $\text{Nd}_{0.5}\text{Sr}_{0.5}\text{MnO}_3$ showing the various atomic coordinates.

The space group is found to be $Imma$. The parameters agree with those reported by Eremenko *et al.*¹⁵ for NSMO 0.5 crystals obtained from the Warwick group and from the Institute of Physics of the Polish Academy of Sciences.

The temperature dependence of ac susceptibility (χ') and resistivity measurements on the crystal were reported in Ref. 6. The paramagnetic insulator to ferromagnetic metal transi-

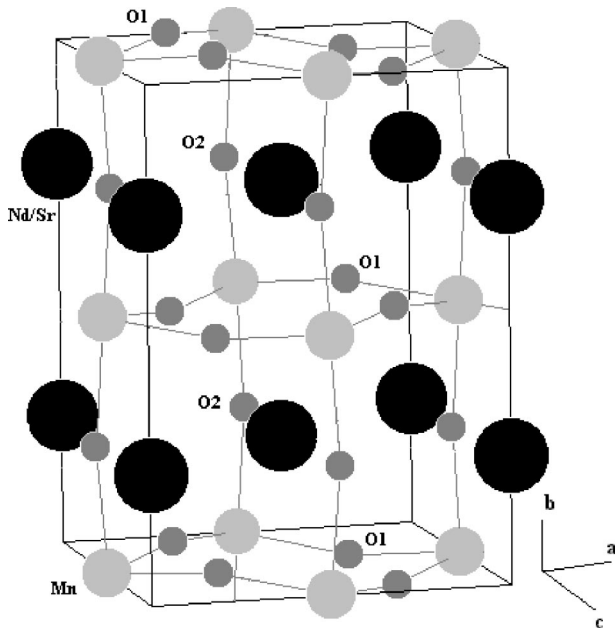


FIG. 1. Structural diagram of $\text{Nd}_{0.5}\text{Sr}_{0.5}\text{MnO}_3$ showing the various atomic coordinates. Layers of the inequivalent oxygens O1 and O2 alternate in the a - c plane.

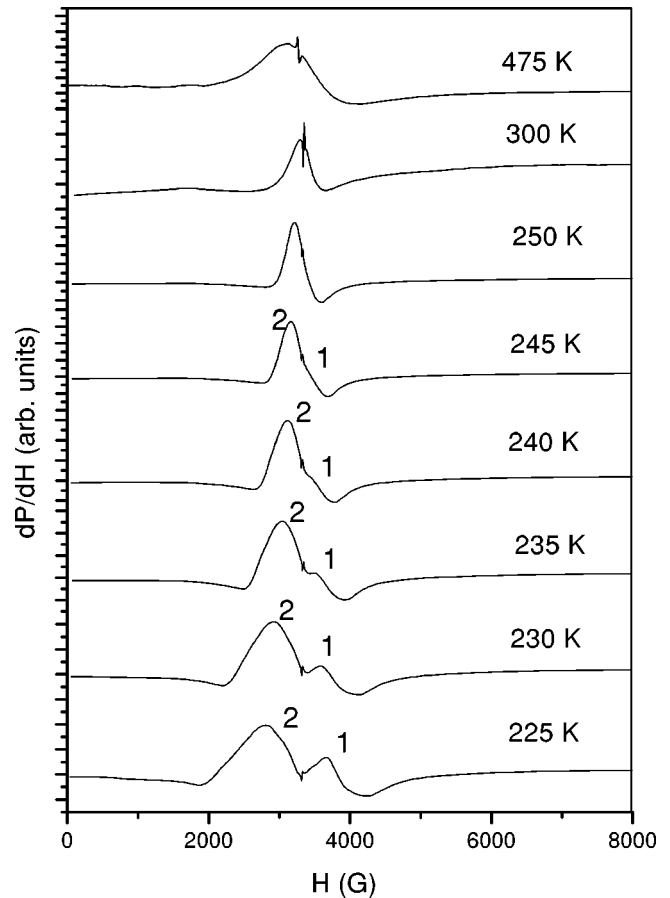


FIG. 2. Representative ESR spectra in the paramagnetic state and between 250 K and 225 K.

tion occurs at 245 K (T_C). The antiferromagnetic transition around 148 K (T_{CO}) is accompanied by a sharp transition to the insulating state.

ESR measurements were performed using a Varian E-112 continuous wave spectrometer at x-band frequency (≈ 9.35 GHz), equipped with a continuous gas-flow cryostat (nitrogen). A spherically shaped crystal of diameter ~ 1 mm was used for the measurement. The orientation of the crystal was determined using a Laue camera in back-scattering geometry. The spectra were recorded with the c axis of the crystal aligned parallel to the applied magnetic field. A platinum resistance thermometer and a heater, kept below the sample, were used to measure and control the temperature from 100 K to 425 K. 2,2-diphenyl(picryl hydrazyl) (DPPH) was used as g marker. The ESR spectra were recorded as the temperature was decreased from 425 K. The angular dependence of the resonance was measured by rotating the sample with respect to an axis perpendicular to the magnetic field at various temperatures.

III. RESULTS AND DISCUSSION

Figures 2, 3, and 4 show ESR spectra in the different temperature ranges. A single line was observed in the paramagnetic state whose shape is asymmetric. When the temperature is reduced below 250 K ($= T_C$), the spectrum splits

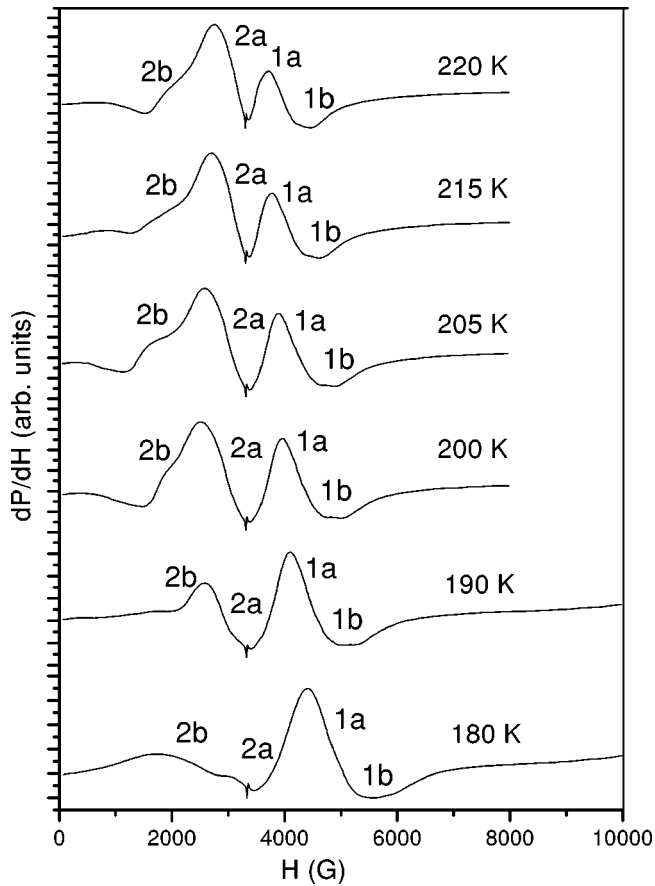


FIG. 3. ESR spectra in the temperature range from 220 K to 180 K.

and the lines broaden. The prominent peak shifts towards lower fields and an additional line appears in the form of a shoulder on the high-field side of the prominent peak. At 225 K, the prominent line which shifts towards lower fields further splits into two and both the lines shift to lower fields down to 180 K. A small shoulder appears in the high-field line also. It was difficult to record the spectrum below 130 K.

The asymmetric spectra were analyzed by fitting to line shapes of the form:¹⁶

$$\frac{dP}{dH} = \frac{d}{dH} \left[\frac{\Delta H + \alpha(H - H_0)}{(H - H_0)^2 + \Delta H^2} \right]. \quad (1)$$

This is an asymmetric Lorentzian line, which includes both absorption and dispersion, where α denotes the dispersion-to-absorption ratio. Such asymmetric line shapes are usually observed in metals for samples whose dimensions are large compared to the skin depth, because the skin effect drives the magnetic component of the microwave field in the sample out of phase and therefore leads to an admixture of dispersion into the absorption spectra. Two or three asymmetric Lorentzians [Eq. (1)] were used to fit the experimental data at various temperature ranges. Figure 5 shows the fits of the experimental data along with the resolved lines. The temperature evolution of the spectra in various temperature regions is discussed below.

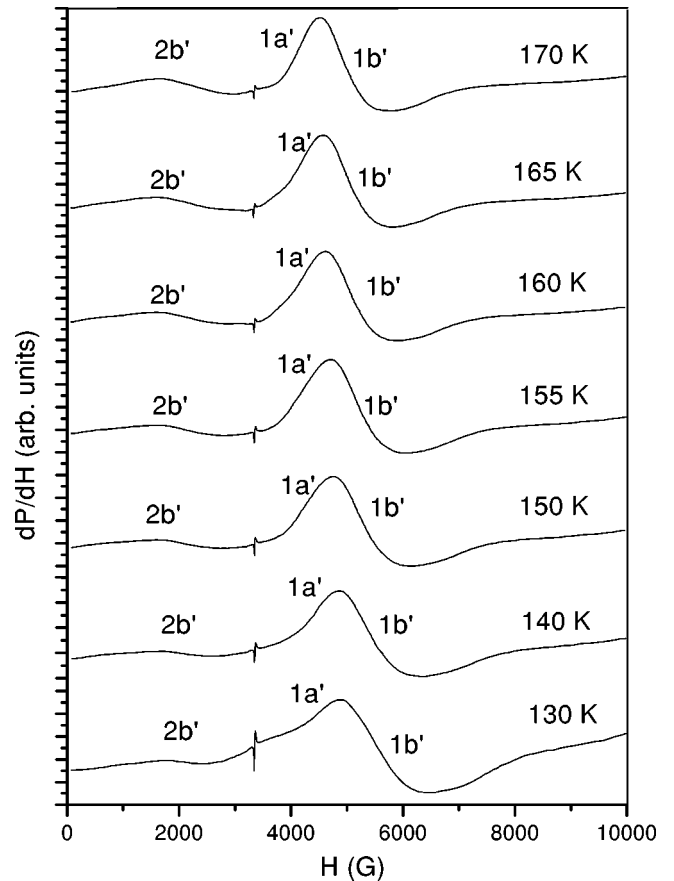


FIG. 4. ESR spectra in the temperature range from 170 K to 130 K.

A. Paramagnetic state: $T > 250$ K

In the paramagnetic state the resonance field, linewidth, and intensity of the ESR spectra were derived by fitting to Eq. (1). Figure 6 shows the resonance field (H_0) derived from fits over the entire temperature range from room temperature down to 130 K. The ESR signal in manganites may be taken to originate from Mn^{4+} ions, because Mn^{4+} ($3d^3$ with $S = 3/2$) ions are expected to have an isotropic g value of ~ 1.99 in an octahedral crystal field. Mn^{3+} ($3d^4$ with $S = 2$) is unlikely to have an observable ESR signal since it has a large zero-field splitting and short spin-lattice relaxation time.¹⁷ The g value of our sample, calculated with respect to the DPPH line, is found to increase with decreasing temperature in the paramagnetic state from 1.80 at 425 K to 1.96 at 250 K (Fig. 7) suggestive of spin correlations above T_C .

A neutron-diffraction study by Kawano *et al.*¹⁸ on NSMO 0.5 points to the existence of two-dimensional dynamical spin correlations induced by orbital ordering in the paramagnetic state. Further insight into the nature of these spin correlations can be obtained by referring to reported ESR spectra on manganites in which the charge ordering transition temperature is higher than the antiferromagnetic transition, (e.g., $\text{Nd}_{0.5}\text{Ca}_{0.5}\text{MnO}_3$, $T_{CO} = 240$ K and $T_N = 140$ K), since this allows us to determine the influence of orbital degrees of freedom. Below T_{CO} , the g value exhibits a prominent in-

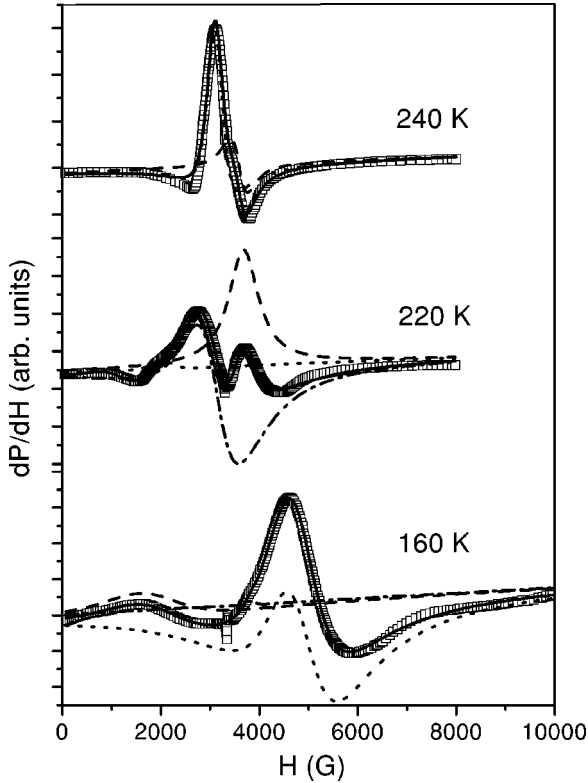


FIG. 5. Representative spectra with fitted and resolved curves at various temperature ranges. The solid lines are the fitted curves and the dashed and dotted lines are resolved curves.

crease and this has been attributed to the development of orbital-ordering.¹⁹ The effect of orbital degrees of freedom on the g value has been studied recently in LiCuVO_4 .²⁰ The presence of such orbitally ordered clusters may similarly give rise to an increase in the g value when the sample is cooled towards T_C .

Based upon the above results, the observed increase in the g value upon cooling in the paramagnetic state in NSMO 0.5 is attributed to orbitally ordered spin clusters. Thus orbital degrees of freedom have an appreciable influence on the na-

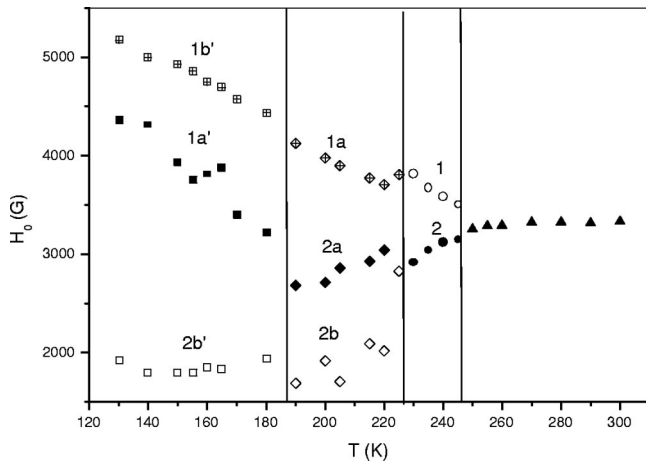


FIG. 6. Plot of resonance field vs temperature of NSMO 0.5 crystal.

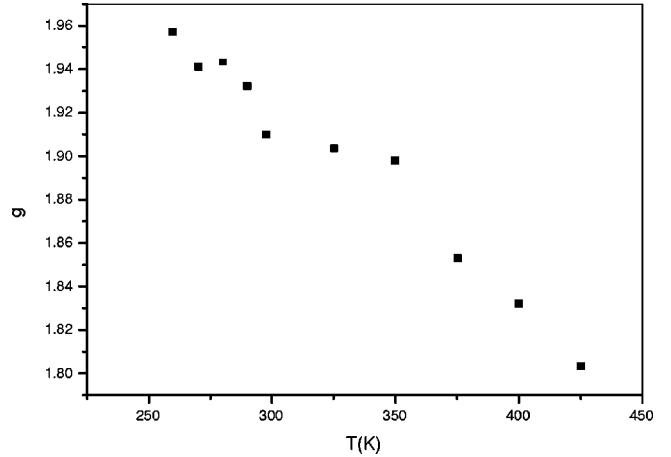


FIG. 7. Plot of g vs temperature in the paramagnetic state.

ture of these spin correlations in manganites even in the paramagnetic state.

The ESR spectrum shows a Dysonian line shape characteristic of a metal up to 475 K.²¹ The A/B ratio of the sample is around 3. To check whether the skin effect is the reason for the asymmetric line shape in the paramagnetic state, we estimate the skin depth $\delta = \sqrt{2\rho/\mu\omega}$ where ρ is the electrical resistivity and ω is the microwave frequency. Using $\rho = 5.0 \times 10^{-5} \Omega\text{m}$ (dc resistivity of single crystal at 295 K), we find the skin depth $\delta = 0.03$ mm which is much less than the sample size of 1 mm. We measured ESR on the crushed powder of the crystal and found a symmetric Lorentzian line down to T_C . This shows that the skin depth of the crystal is responsible for observed asymmetric line shape.

The paramagnetic linewidth (ΔH_{pp}) is found to increase in a quasilinear manner with increase of temperature above T_C (Fig. 8). It goes through a minimum at 270 K ($\approx 1.1T_C$), as the temperature decreases and below which it increases again (inset of Fig. 8). The linewidth behavior above T_C could be described by an equation of the form:²²

$$\Delta H_{pp}(T) = \Delta H_{pp}(\infty) \left[\frac{C}{T\chi} \right], \quad (2)$$

where C/T is the single-ion (Curie) susceptibility, χ is the measured paramagnetic susceptibility and $\Delta H_{pp}(\infty)$ is the linewidth expected at temperatures high enough for the dc susceptibility to follow a Curie-Weiss law. Such a dependence accounts for the quasilinear behavior near T_C and the tendency to saturation at higher temperatures in manganites resulting in a *universal* temperature dependence of the ESR linewidth in a scale normalized to T_C . This is attributed to the existence of magnetic clusters well above T_C . The observed temperature dependence of the linewidth supports the existence of orbitally ordered spin clusters inferred from the temperature dependence of the paramagnetic g value.

Figure 8 shows the linewidth plotted accordingly on this universal curve in a normalized scale T/T_C . $\Delta H_{pp}(\infty)$ was calculated by fitting to this universal curve and was found to be 2400 G. This value of $\Delta H_{pp}(\infty)$ is of the same order as the values of 2600 G for La and 4500 G for Pr-Sr

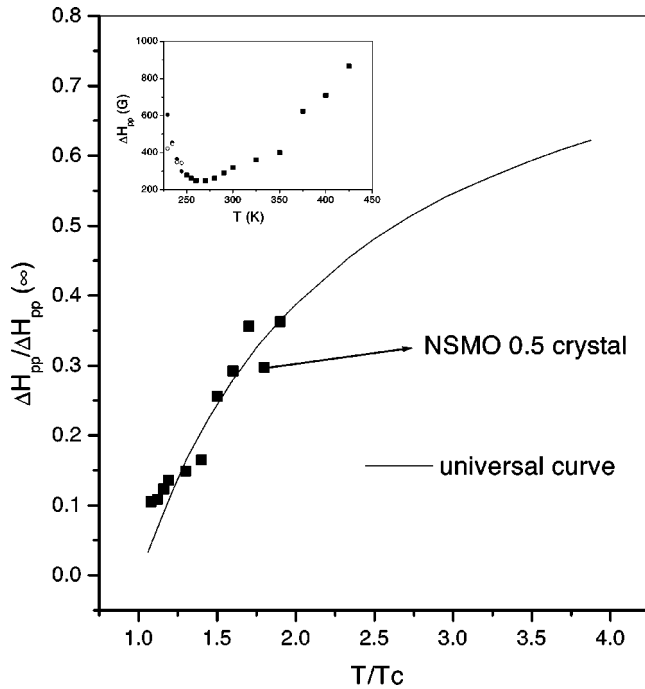


FIG. 8. Plot of $\Delta H_{pp}/\Delta H_{pp}(\infty)$ vs T/T_C in the paramagnetic state. The continuous line shows the theoretical curve of Eq. (2). Inset shows the minimum in ΔH_{pp} at 270 K.

manganites.²² The single-crystal value is about the same (2500 G) as for polycrystalline NSMO 0.5 reported by us earlier.⁹

The ESR intensity is another important parameter which can be used to identify the nature of the ions contributing to the resonance in the paramagnetic state. The intensity of the ESR spectrum, which is proportional to the number of paramagnetic spins, is the area under the absorption curve. There are two different methods of calculation of the intensity of first derivative ESR spectrum. One is the double integration of the observed ESR spectrum. In another method, the intensity of the ESR line may be obtained from the following expression:

$$I \propto [\Delta H_{pp}]^2 Y', \quad (3)$$

where $2Y'$ is the peak-to-peak derivative amplitude.

As the spectra are asymmetric in the NSMO 0.5 crystal, the second method is adopted to calculate the intensity. The intensity is given by $I = \eta \chi_{esr} \omega Q_L$ for small samples. Then the intensity is multiplied by a constant, proportional to the quality factor and dimension of the cavity, to determine χ_{esr} . The result is shown in Fig. 9 along with χ_{dc} . The contribution to the susceptibility due to the Nd ions is subtracted from χ_{dc} . It shows that both the susceptibilities follow the same temperature dependence. This is similar to the behavior observed in $\text{La}_{0.67}\text{Ca}_{0.33}\text{MnO}_3$.²² This clearly indicates all the Mn ions contribute to the observed ESR spectra.

To account for the temperature dependence of the ESR signal of manganites in the paramagnetic state, Shengelaya *et al.*²³ used the “bottleneck” mechanism and assigned the ESR signal to Mn^{4+} ions with a ferromagnetic Curie-Weiss-like behavior arising from the ferromagnetic coupling be-

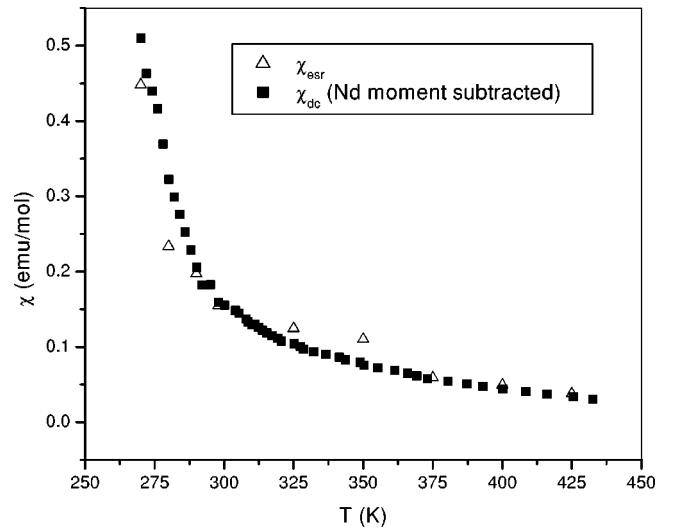


FIG. 9. Plot of susceptibility vs temperature above T_C .

tween the Mn^{3+} and Mn^{4+} subsystems. However the ESR intensity variation has been fitted by them only over a small temperature range above T_C (up to $\sim 2T_C$) and there are deviations above this interval. Causa *et al.*²² correlated this deviation with the tendency to saturation of ΔH_{pp} as shown by the universal temperature dependence for manganites (Fig. 8). In this model the ESR signal is assigned to spin clusters of both Mn^{3+} and Mn^{4+} ions and is found to agree with the observed temperature dependence of the ESR spectrum well above T_C (up to $\sim 4T_C$). Hence this model is used in the present analysis.

B. Ferromagnetic state: 230 K < T < 245 K

Between 245 K and 230 K, an equation consisting of two asymmetric Lorentzian terms [Eq. (1)] was used to fit the data. A new line (line 1) develops at 245 K as a shoulder on the high-field side. The temperature at which the line splits, viz., 245 K coincides with T_C obtained from magnetization. The shifts of the two lines upon cooling are in opposite direction: the prominent line (line 2) shifts to lower fields whereas line 1 shifts to higher fields.

The observed two line feature in the ferromagnetic state is attributed to coexisting ferromagnetic and para/antiferromagnetic phases as in the case of polycrystalline $\text{La}_{0.5}\text{Ca}_{0.5}\text{MnO}_3$ and $\text{Nd}_{0.5}\text{Sr}_{0.5}\text{MnO}_3$ manganites.^{9,24,25} In a single crystal, this line splitting could also be due to the magnetocrystalline anisotropy of the sample, when the field is not applied along the easy direction of magnetization. This can be checked by the angular variation of the ESR spectrum. If the line splitting is due to the coexisting phases, there should be no significant angular variation, whereas the magnetocrystalline anisotropy of the sample induces a periodic variation of the resonance field depending on the direction of orientation of the crystallographic axes with respect to the applied magnetic field. If K_1 is the anisotropy constant and M_0 the saturation magnetization at a given temperature, then resonance occurs at two fields above and below a critical field, called the effective anisotropy field, H_{an}

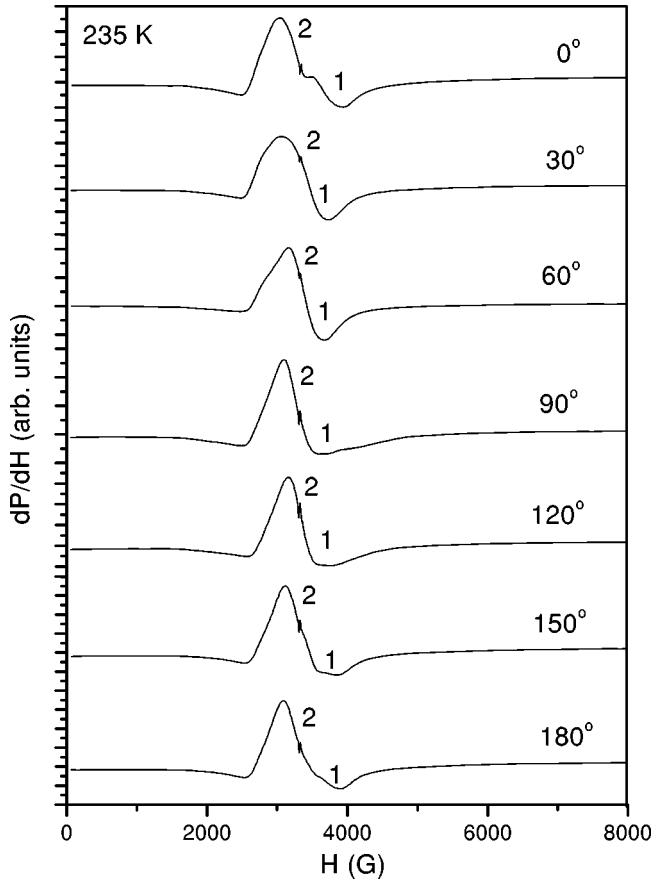


FIG. 10. Angular variation of ESR spectra at 235 K.

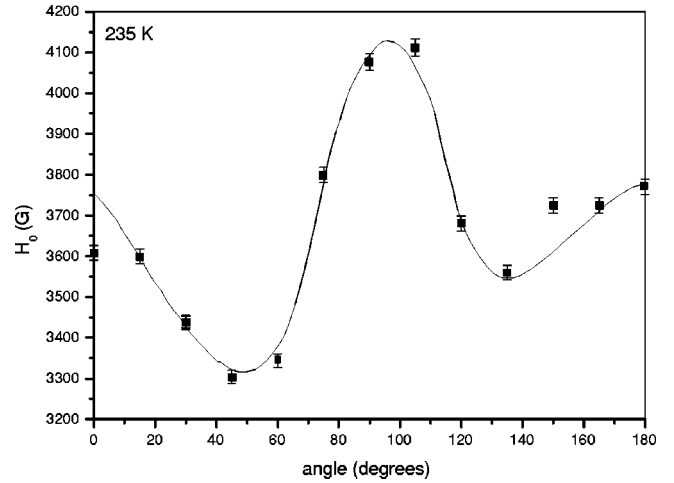
$=2K_1/M_0$.²⁶ This field is a virtual magnetic field, whose action on the magnetization is equivalent to the effect of real interaction forces responsible for the anisotropy. If we can find such an anisotropy field H_{an} , then the equation of motion, whose solution gives the susceptibility tensor, is of the form:

$$\frac{d\mathbf{M}}{dt} = -\gamma\mathbf{M} \times (\mathbf{H} + \mathbf{H}_{an}) + \omega_r[\chi_0(\mathbf{H} + \mathbf{H}_{an}) - \mathbf{M}]. \quad (4)$$

We shall assume the dependence of \mathbf{H}_{an} on \mathbf{M} to have the form: $\mathbf{H}_{an} = -\mathbf{N}^{an}\mathbf{M}$ where \mathbf{N}^{an} is the magnetocrystalline anisotropy tensor.

In order to investigate the origin of the two resonance lines below T_C , angular dependent ESR measurements of the NSMO 0.5 crystal were made. The spherical shape of the sample nullifies the demagnetizing effects. Figures 10 and 11 show the angular variation of the line shape and of the resonance position of the high-field line at 235 K, respectively. The variation is $\cos 4\phi$ with maxima at 0° , 90° , and 180° and minima at 45° and 135° . This resembles the dependence of the resonance field on the angle ϕ between applied field (H) and the $[100]$ axis in the (010) plane for a cubic crystal. For $H_0 \gg K_1/M_0$, the angular variation of the resonance field is approximately given by²⁶

$$H_0 = \frac{\omega}{\gamma} - \frac{K_1}{2M_0} \left(\frac{3}{2} - \frac{5}{2} \cos 4\phi \right). \quad (5)$$

FIG. 11. Plot of resonance position of the high-field line vs angle between applied field H and the axis $[100]$ in the (010) plane at 235 K. The solid line is guide to eye.

Octahedral (MnO_6) tilts reduce the symmetry from cubic to orthorhombic in perovskite manganites. For small octahedral tilts the unit cell of NSMO 0.5 may be thought of as a “pseudocube” (with local $Imma$ symmetry). This is borne out from the angular variation of the resonance field (Fig. 11). Thus the two-line feature observed in this temperature interval is explained by invoking the presence of magnetocrystalline anisotropy and its presence is confirmed by measuring the angular variation of the resonance field.

The fact that the two-line spectrum originates from the magnetocrystalline anisotropy can be explained in the following way. During a typical field sweep in the ESR experiment, if the field is not applied along the easy axis of magnetization (as in the present case) and when the magnetization is far from saturation, the magnetization of the specimen aligns along the easy direction for small values of the field, resulting in a low-field resonance line. Upon further increasing the field, the spins tend to align along the direction of the applied field resulting in the high-field resonance line. Thus the anisotropy field splits the observed ferromagnetic resonance (FMR) signal. If the two lines originate from magnetocrystalline anisotropy when the sample is not oriented along the easy axis of magnetization, then spectra measured at fields sufficiently high to magnetize the sample completely along the field direction should show a single line. This was verified by Q -band ESR measurements. A single line appears over the entire temperature range from 400 K to 130 K. This shows that the magnetic field of 12 500 G for Q -band measurements is sufficient to magnetize the sample completely in the field direction and that this field is greater than the anisotropy field, H_{an} . A typical Q -band ESR spectrum recorded at 200 K is shown in Fig. 12.

Mahendiran *et al.*²⁷ have reported magnetization versus field curves below T_C in NSMO 0.5. The “knee” point occurs around 5000 G. Thus in a typical X-band field scan from 0–8000 G, two resonance lines are expected when the sample is not oriented along the easy direction. The Q -band resonance field (~ 35 GHz, ~ 12 500 G) is beyond the knee point in the magnetization curve for NSMO 0.5 and hence

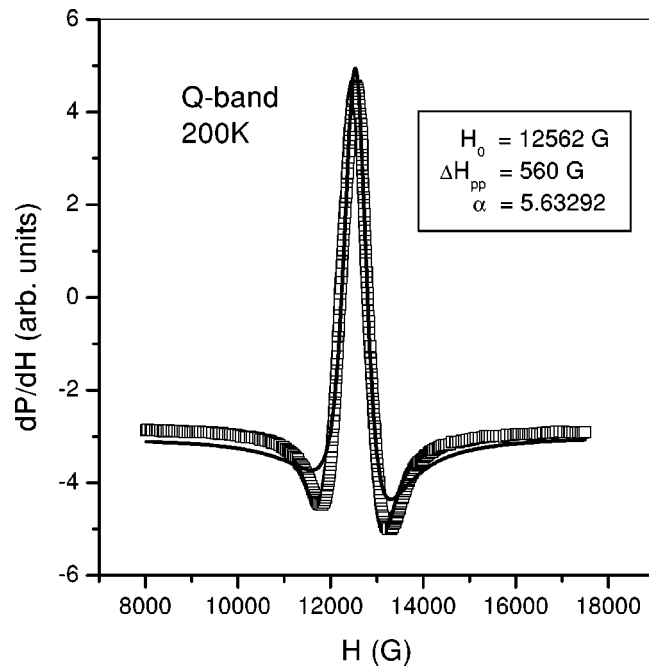


FIG. 12. Q -band ESR spectrum recorded at 200 K. Solid line is a fit to an asymmetric Lorentzian line [Eq. (1)].

only one resonance line is observed irrespective of sample direction. Thus the angular variation of the resonance field (Fig. 11), the observed X - and Q -band spectra and reported M - H data²⁷ confirm that the anisotropy field plays an important role in determining the temperature dependence of the ESR spectrum below T_C .

C. 180 K < T < 225 K

Below 225 K, both line 1 and line 2 split further into two lines each (Fig. 3). One of the split components of line 1 (1b) was too weak to be analyzed and its temperature dependence is not discussed any further. However it is prominently observed when the angular variation of the line shape was recorded at 180 K (Fig. 13). This splitting could be due to the A -type antiferromagnetic state, which is found to coexist with the ferromagnetic state below 225 K observed by Ritter *et al.* from neutron diffraction.⁷

Figures 13 and 14 show the angular variation of the line shape and of the resonance fields, respectively, at 180 K. The resonance field has a $\cos 4\phi$ angular variation with maxima at 0° , 90° , and 180° and minima at 45° and 140° similar to the data obtained at 235 K. The observed $\cos 4\phi$ behavior of lines 1a and 1b indicates the existence of two different values for the anisotropy field in this temperature region. The deviation from $\cos 4\phi$ behavior of the angular dependencies is possibly due to the deviation from cubic symmetry and magnetic inhomogeneities.

Thus the observed splitting of lines 1 and 2 below 225 K points to the presence of ferromagnetic heterogeneity with two different magnetocrystalline anisotropies arising from the onset of A -type antiferromagnetic order, i.e., the pairs of lines [1a, 2a, 1b] (not shown in Fig. 6), and 2b] originate from two different anisotropy fields and is attributed to the pres-

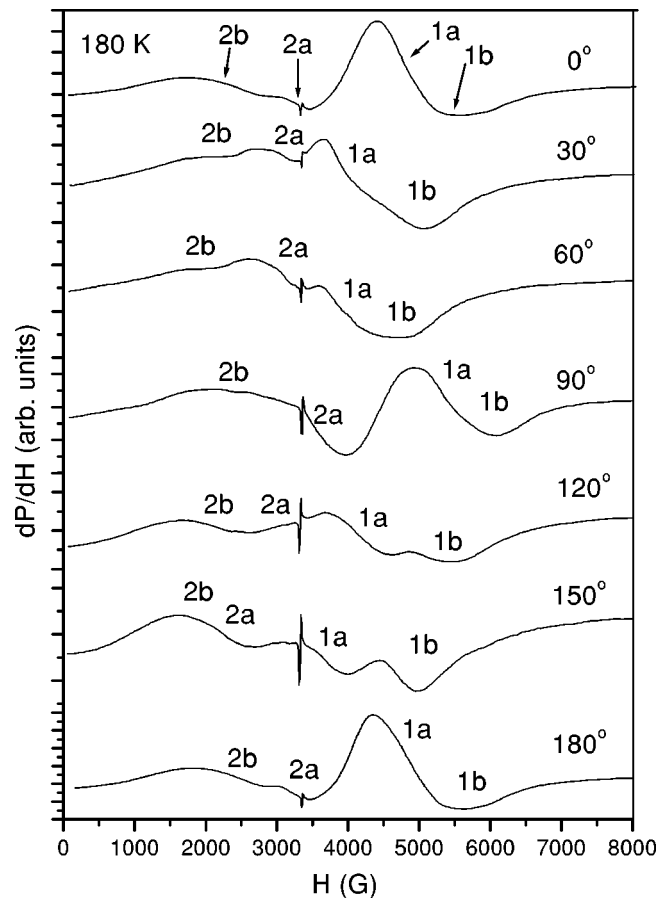


FIG. 13. Angular variation of ESR spectra at 180 K.

ence of the A -type AFM phase. The observation of ferromagnetic-like feature for the coexisting A -type antiferromagnetic phase arises from the canted spins having non-zero net magnetization possibly with easy axis of magnetization away from the magnetization direction of the dominant ferromagnetic phase.

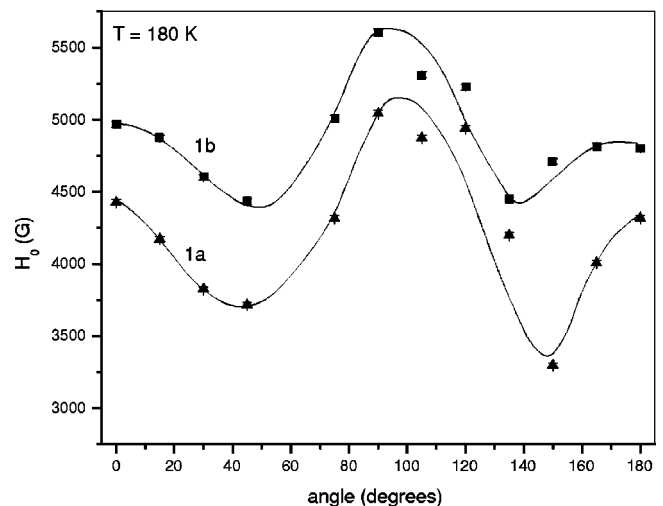


FIG. 14. Plot of resonance field vs angle between H_0 and the axis [100] in the (010) plane at 180 K. The solid lines are guides to the eye.

D. $T < 180$ K

Below 180 K, the resolution between lines 1a and 2a decreases markedly and a single asymmetric line is observed, line 2b still being present at low fields. The intensity of the lines is nearly constant down to the charge ordering temperature T_{CO} (148 K). However satisfactory line shape fits in this temperature region could be obtained only if three asymmetric Lorentzians are used. Therefore the peak positions obtained from the fits are labeled as 1a', 1b', and 2b' (Fig. 6) to represent this change in the line shape. This change in line shape coincides with the onset of the CE state below 180 K, as shown by Ritter *et al.*⁷ Since four resonance lines are observed well below T_{CO} , we infer that FM and A-type AFM phases coexist with the CO phase. This suggests that the transition to the CO is gradual in agreement with ⁵⁵Mn NMR data.⁶

IV. CONCLUSION

The temperature dependence of the g value, linewidth, and intensity above T_C point to the existence of orbitally ordered spin clusters of both Mn^{3+} and Mn^{4+} ions in the paramagnetic state. Thus orbital degrees of freedom have an appreciable influence on the dynamical spin correlations in manganites even in the paramagnetic state. The magnetocrystalline anisotropy is found to split the resonance line into

two below T_C . This is confirmed by $\cos 4\phi$ angular dependence of the resonance field and the Q -band spectra. Both FMR lines further split into two each below 225 K. This splitting is attributed to the presence of two different anisotropy fields which may arise from the onset of A-type AFM ordering. The existence of two types of anisotropy fields was confirmed by $\cos 4\phi$ angular dependence of the resonance fields.

In summary, our electron magnetic resonance study of NSMO 0.5 single crystal shows the complex nature of the paramagnetic phase and the temperature evolution of coexisting ferromagnetic and A-type antiferromagnetic phases in the interval 245–180 K, which can be explained from variations in magnetocrystalline anisotropy.

ACKNOWLEDGMENTS

The authors thank Dr. G. Balakrishnan, Department of Physics, University of Warwick, UK, for providing the NSMO 0.5 crystal used in this study, N. Sivaramakrishnan, Regional Sophisticated Instrumentation Center, IIT Madras, for assistance in ESR measurements and Dr. Babu Varghese, Regional Sophisticated Instrumentation Center, IIT Madras for the single-crystal x-ray diffraction measurement and discussions.

*Electronic address: rajan@acer.iitm.ernet.in

¹A.P. Ramirez, *J. Phys.: Condens. Matter* **9**, 8171 (1997).

²P.G. Radaelli, D.E. Cox, M. Marezio, and S.-W. Cheong, *Phys. Rev. B* **55**, 3015 (1997).

³E. Dagotto, T. Hotta, and A. Moreo, *Phys. Rep.* **344**, 1 (2001).

⁴N. Fukumoto, S. Mori, N. Yamamoto, Y. Moritomo, T. Katsufuji, C.H. Chen, and S.-W. Cheong, *Phys. Rev. B* **60**, 12 963 (1999).

⁵G. Papavassiliou, M. Fardis, M. Belesi, I. Panagiotopoulos, G. Kallias, D. Niarchos, C. Dimitropoulos, and J. Dolinsek, *Phys. Rev. Lett.* **84**, 761 (2000).

⁶M. Pattabiraman, P. Murugaraj, G. Rangarajan, C. Dimitropoulos, J-Ph. Ansermet, G. Papavassiliou, G. Balakrishnan, D.McK. Paul, and M.R. Lees, *Phys. Rev. B* **66**, 224415 (2002).

⁷C. Ritter, R. Mahendiran, M.R. Ibarra, L. Morellon, A. Maignan, B. Raveau, and C.N.R. Rao, *Phys. Rev. B* **61**, R9229 (2000).

⁸T.Y. Koo, V. Kiryukhin, P.A. Sharma, J.P. Hill, and S.-W. Cheong, *Phys. Rev. B* **64**, 220405 (2001).

⁹S. Angappane, G. Rangarajan, and K. Sethupathi, *J. Appl. Phys.* **93**, 8334 (2003).

¹⁰Enraf-Nonius CAD-4 software, Version 5.0 (Enraf-Nonius, Delft, The Netherlands, 1989).

¹¹A.C.T. North, D.C. Phillips, and F.S. Mathews, *Acta Crystallogr., Sect. A: Cryst. Phys., Diffr., Theor. Gen. Crystallogr.* **A24**, 351 (1968).

¹²G. M. Sheldrick, SHELXL97 and SHELXS97 (University of Gottigen, Germany, 1997).

¹³A. L. Spek, PLATON for Windows (Utrecht University, The Netherlands, 1999).

¹⁴C. K. Johnson, Oak Ridge National Laboratory Report No. ORNL-5138, 1976 (unpublished).

¹⁵V. Ereman, S. Gnatchenko, N. Makedonska, Yu. Shabakayeva,

M. Shvedun, V. Sirenko, J. Fink-Finowicki, K.V. Kamenev, and G. Balakrishnan, *Low Temp. Phys.* **27**, 930 (2001).

¹⁶V.A. Ivanshin, J. Deisenhofer, H.-A. Krug von Nidda, A. Loidl, A.A. Mukhin, A.M. Balbashov, and M.V. Eremin, *Phys. Rev. B* **61**, 6213 (2000).

¹⁷A. Abragam and B. Bleaney, *Electron Paramagnetic Resonance of Transition Ions* (Clarendon Press, Oxford, 1970).

¹⁸H. Kawano-Furukawa, R. Kajimoto, H. Yoshizawa, Y. Tomioka, H. Kuwahara, and Y. Tokura, *Phys. Rev. B* **67**, 174422 (2003).

¹⁹Janhavi P. Joshi, Rajeev Gupta, A.K. Sood, S.V. Bhat, A.R. Raju, and C.N.R. Rao, *Phys. Rev. B* **65**, 024410 (2002).

²⁰H.-A. Krug von Nidda, L.E. Svistov, M.V. Eremin, R.M. Eremina, A. Loidl, V. Kataev, A. Validov, A. Prokofiev, and W. Assmus, *Phys. Rev. B* **65**, 134445 (2002).

²¹F.J. Dyson, *Phys. Rev.* **98**, 349 (1955).

²²M.T. Causa, M. Tovar, A. Canerio, F. Prado, G. Ibanez, C.A. Ramos, A. Butera, B. Alascio, X. Obradors, S. Pinol, F. Rivadulla, C. Vazquez-Vazquez, M.A. Lopez-Quintela, J. Rivas, Y. Tokura, and S.B. Oseroff, *Phys. Rev. B* **58**, 3233 (1998).

²³A. Shengelaya, Guo-Meng Zhao, H. Keller, and K.A. Muller, *Phys. Rev. Lett.* **77**, 5296 (1996).

²⁴F. Rivadulla, M. Freita-Alvite, M.A. Lopez-Quintela, L.E. Huesa, D.R. Miguens, P. Sande, and J. Rivas, *J. Appl. Phys.* **91**, 785 (2002).

²⁵Janhavi P. Joshi, A.K. Sood, S.V. Bhat, A.R. Raju, and C.N.R. Rao, cond-mat/0201336 (unpublished).

²⁶A. G. Gurevich, *Ferrites at Microwave Frequencies* (Consultants Bureau, New York, 1963).

²⁷R. Mahendiran, M.R. Ibarra, A. Maignan, F. Millanage, A. Arulraj, R. Mahesh, B. Raveau, and C.N.R. Rao, *Phys. Rev. Lett.* **82**, 2191 (1999).